HOSTED BY

ELSEVIER

Available online at www.sciencedirect.com

ScienceDirect

Soils and Foundations xxx (xxxx) xxx

SOILS AND FOUNDATIONS

www.elsevier.com/locate/sandf

Technical Paper

Centrifuge modelling of the behaviour of pile groups under vertical eccentric load

L. de Sanctis [a], R. Di Laora [b,*], T.K. Garala [c], S.P.G. Madabhushi [c], G.M.B. Viggiani [c], P. Fargnoli [d]

[a] *University of Napoli Parthenope, Napoli, Italy*
[b] *University of Campania Luigi Vanvitelli, Aversa, Italy*
[c] *University of Cambridge, Cambridge, UK*
[d] *Enel Green Power, Roma, Italy*

Received 1 July 2020; received in revised form 22 November 2020; accepted 17 January 2021

Abstract

Annular shaped pile groups are a very common foundation layout for onshore wind turbines and other slender structures. In this study, their performance under vertical loads of moderate to high eccentricity, including moment rotation response and bearing capacity, was investigated by centrifuge testing on small scale physical models embedded in kaolin clay. To identify experimentally the capacity of the examined pile groups under different load paths, the model foundations were loaded monotonically until a clear collapse mechanism was achieved. The testing procedure and the proposed interpretation methodology can be easily adapted to load paths or pile layouts other than those considered in the current study. The experimental data can be adopted as a useful benchmark for mathematical models aimed at predicting the response of pile groups to complex load paths. The results of this testing program can also be used to assess the degree of conservatism of current methods adopted by industry for the design of piled foundations subjected to eccentric loads.

Keywords: Centrifuge modelling; Pile group; Wind turbines; Eccentric loading

1. Introduction

The large demand of tall wind turbines and earthquake resistant structures has led to new research in the field of foundations subjected to complex actions, such as dynamic and cyclic multi-component loads. This has presented a formidable challenge to geotechnical engineering, as current design methods adopted by the industry are often unable to ensure stringent performance requirements with a reasonable level of conservatism. In particular, innovative design solutions for the foundations of wind turbines are required to accommodate the increasing demand of renewable energy. In 2015, the cumulative installed wind capacity across the world has increased by 17% relative to the preceding year (GWEC, 2015). In the USA, for example, the consumption of energy in 2014 was only 1.24% higher than that in the preceding year, while the use of renewable energy increased by 10.8% (Shrestha, 2015). According to Liebreich (2017), the maximum height of wind turbines has grown from 40 to 150 m in the past 30 years, to take advantage of higher wind speed and reduced turbulence at higher altitudes. It is highly probable that the height of wind turbines will increase further in the next decade. As a matter of fact, tall wind turbines are the most convenient choice for the production of wind energy. Since the loads transmitted by a tall tower under extreme

Peer review under responsibility of The Japanese Geotechnical Society.
* Department of Engineering, University of Campania Luigi Vanvitelli, Aversa, Italy

https://doi.org/10.1016/j.sandf.2021.01.006
0038-0806/

wind conditions are remarkably eccentric, the dead load of any shallow foundation has to be large enough to avoid bearing capacity failure or the occurrence of overturning. This usually results into very substantial circular rafts with extremely large thickness and diameter, also referred to in the literature as 'gravity' foundations. In some cases, the dimensions of the required gravity foundation may be above the upper limit of what is possible in practice. In the case of onshore wind turbines, the most frequent alternative is represented by a piled foundation (Ravichandran et al. 2018), even if other options are available, e.g., monopile or caisson foundations, or soil treatment by gravel or grouted columns.

This work focuses on the behaviour of pile groups under moderate to high eccentric vertical loads. Current design methods, see *e.g.*, AASHTO Bridge Design Specification (2012), identify the capacity of a pile group as the eccentric vertical load corresponding to the achievement of the axial capacity of the outermost pile (in compression or in tension). However, this does not correspond to failure of the foundation but rather to the onset of yielding, as the pile group is still capable of carrying further external loads, exploiting the ductility reserves of the system. Past research work has targeted the evaluation of the collapse domain of pile groups from tests on reduced scale models of groups of piles embedded in sand (Kishida & Meyerhof 1965, Meyerhof & Ranjan 1973, Meyerhof et al. 1983) and saturated clay (Saffery & Tate 1961, Meyerhof 1981, Meyerhof & Yalcin 1984). As a result, semi-empirical relationships linking the axial and the moment capacity of pile groups are available (Meyerhof et al. 1983), but their application in practice is not straightforward due to the inherent difficulty in the evaluation of the moment capacity under zero axial load. Di Laora et al. (2019) have recently proposed a novel, exact solution for the interaction diagrams of pile groups, based on the theorems of limit analysis. This allows to evaluate the collapse domain in the (axial load Q, moment M) plane from the axial capacities of the single pile in compression and tension. The predictive capabilities of this approach, however, have not yet been proven experimentally.

Despite the considerable research effort on the topic, the failure mechanism of a pile group under vertical eccentric load is not yet well understood. For instance, the kinematics of the failure mechanism and the evolution of the load distribution among the piles, when the pile group is subjected to load paths with constant eccentricity, e ($=M/Q$), constant axial load, or any other path are still unclear, as most of the existing work addressed solely the definition of the collapse domain.

Finally, pile-to-pile interaction mechanisms have been traditionally investigated under the assumption of positive (compressive) axial load on piles. The early studies on this subject date back to Poulos (1968), Butterfield & Banerjee (1971) and Banerjee & Driscoll (1976). Since then, a number of comprehensive works have been published, including well-documented case history of instrumented piled rafts (Clancy & Randolph 1993, Russo & Viggiani 1998, de Sanctis & Russo 2008). As outlined by Viggiani et al. (2012), this research effort has led to satisfactory procedures of analysis for the prediction of settlements of piled foundations. However, there is a dearth of experimental observations on the rotation of pile groups for load distributions involving negative (tension) axial loads, in which pile-to-pile interaction under tensile axial loads may play a significant role.

In the light of the above, the aims of this research are twofold: (i) to define a standard procedure to evaluate the moment rotation response of small pile groups under vertical and eccentric load using centrifuge testing; (ii) to provide well-documented experimental evidence on the critical issue of the bearing capacity of piled foundations under loads with moderate to high eccentricity, involving tension load in piles. These data can be usefully adopted as a benchmark for mathematical models aimed at predicting the response of pile groups to different load paths in the (Q, M) plane.

2. Centrifuge modelling of small pile groups

The experimental program was carried out at the Schofield Centre of the University of Cambridge. Two sets of centrifuge tests were performed at an increased gravity of $50g$ on annular shaped pile groups consisting of 8 aluminium piles and isolated single piles embedded in kaolin clay. Fig. 1 illustrates the arrangement of the model foundations in the cylindrical container adopted for the purpose of this study. The first set of experiments, or Set A (Fig. 1a) included a loading test in compression and one in tension on isolated piles, a loading test on the annular group under vertical centred load, and a loading test under highly eccentric vertical load. The second set of experiments, or set B (Fig. 1b) included two loading tests on isolated piles, once again one in compression and one in tension, a loading test on the pile group under a positive (compressive) vertical load with small eccentricity and, finally, a loading test under a negative (tensile) vertical load with small eccentricity.

All model piles were closed-ended hollow cylinders, with a thickness of 1 mm (50 mm at prototype scale), an outer diameter of 10 mm (0.5 m at prototype scale), and a length of 280 mm (14 m at prototype scale). They were embedded in the kaolin clay layer for 240 mm, with the exception of the isolated piles for tests in tension, whose embedded length was 250 mm, so as to make the shaft capacity in tension comparable to that in compression even under large uplift displacements. Isolated piles were connected to square rafts with a width of 40 mm and a thickness of 10 mm. The 8 piles in the annular groups were always arranged according to the same layout, equally spaced and with their centres along a circle with a diameter of 120 mm. They were connected with spherical hinges to an aluminium circular raft with a diameter of 138 mm, which was clear of the soil (Fig. 2). The dimensions in Figs. 1 and

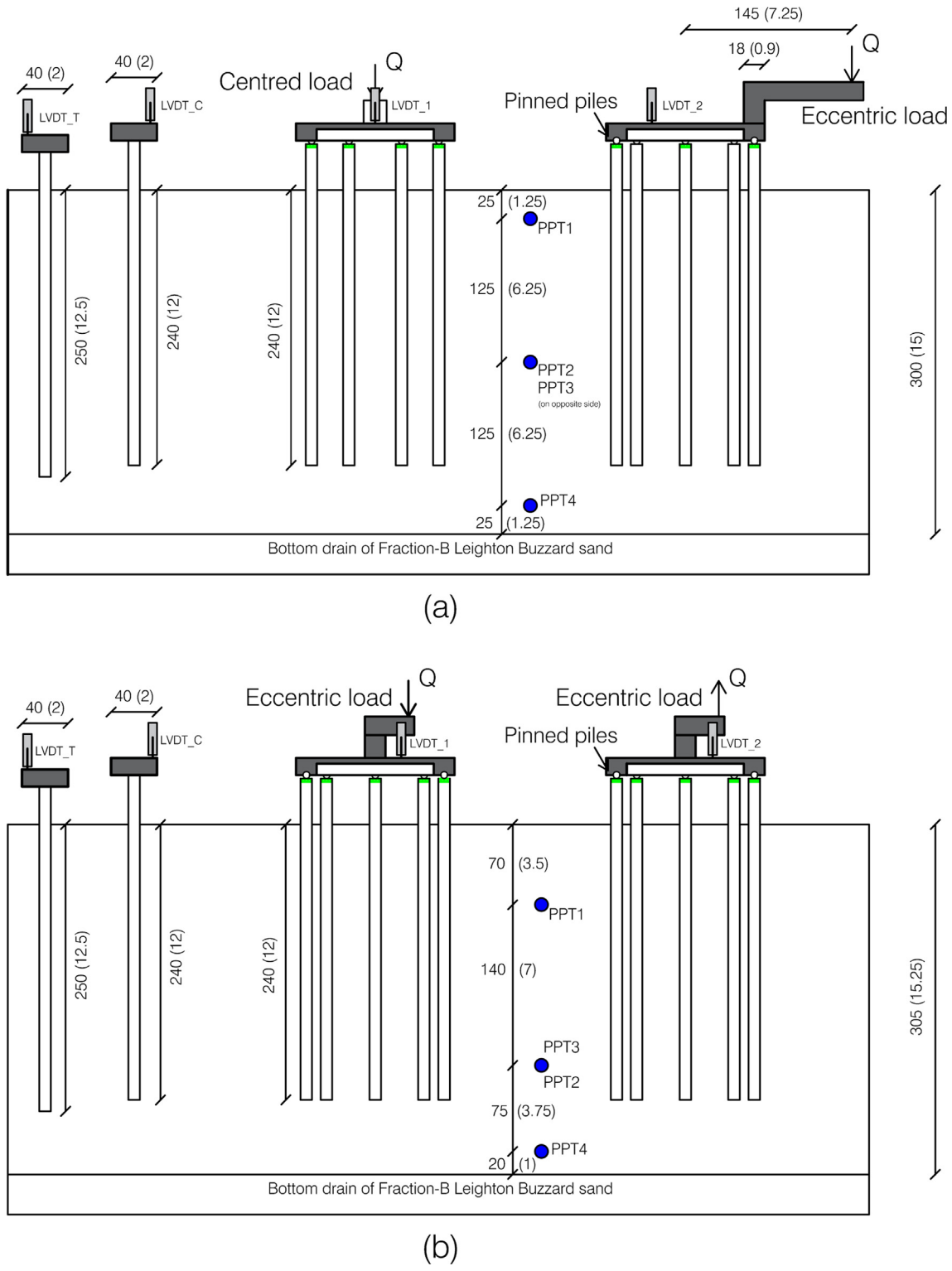

Fig. 2. Schematic cross sections of foundation models in experiment sets A and B; dimensions are given in mm at model scale, while dimensions in brackets (in m) refer to prototype scale.

2 are at model scale and the values in parentheses represent the prototype dimensions. A skirted connecting raft was adopted to minimize the axial load carried by piles before the application of the external load, as detailed in the following. The vertical load was applied under constant eccentricity by means of a cantilever beam.

Table 1
Properties of speswhite kaolin clay (Lau, 2015).

Plastic limit, PL (%)	30
Liquid limit, LL (%)	63
Plasticity Index, PI (%)	33
Specific gravity, G_s	2.6
Slope of critical state line (CSL) in q-p' plane, M	0.9
Slope of unloading-reloading line, κ	0.039
Intercept of CSL at p'=1 kPa, Γ	3.31
Slope of normal compression line, λ	0.22

2.1. Models preparation and experimental setup

The model foundations were inserted in the layer of clay within a cylindrical container with a diameter of 850 mm (42.5 m at prototype scale) and a height of 400 mm (20 m at prototype scale), as shown in Figs. 1 and 2. The clay was underlain by a thin layer of dense fraction-B Leighton Buzzard sand (mean particle size, D_{50} = 0.80 mm), to allow drainage at the bottom of the model during the consolidation stage. A porous Vyon plastic sheet and a filter paper were also placed on top of the sand to avoid the passage of clay through the drainage boundary. The clay layer was prepared from a slurry obtained mixing speswhite kaolin clay powder and de-aired water at nearly twice the liquid limit. The properties of kaolin clay, extensively used in Cambridge for many experimental campaigns, are listed in Table 1 (Lau, 2015). The clay layer was consolidated at 1g by applying a vertical stress of 70 kPa at the top and a suction of −70 kPa at the base, as shown schematically in Fig. 3. Initially, the cylindrical tub containing the clay slurry was placed under a computer-controlled hydraulic press to consolidate under vertical stress and only at a later stage was a suction applied at the bottom to further consolidate the clay slurry. The purpose and importance of clay consolidation using a combination of vertical stress and suction-induced seepage are explained in detail by Garala & Madabhushi (2019). Fig. 4(a) shows the effective vertical stress profile at the end of the 1g consolidation stage, before removal from the hydraulic press, using the normalized depth, z/H, in which H is the final height of the clay layer.

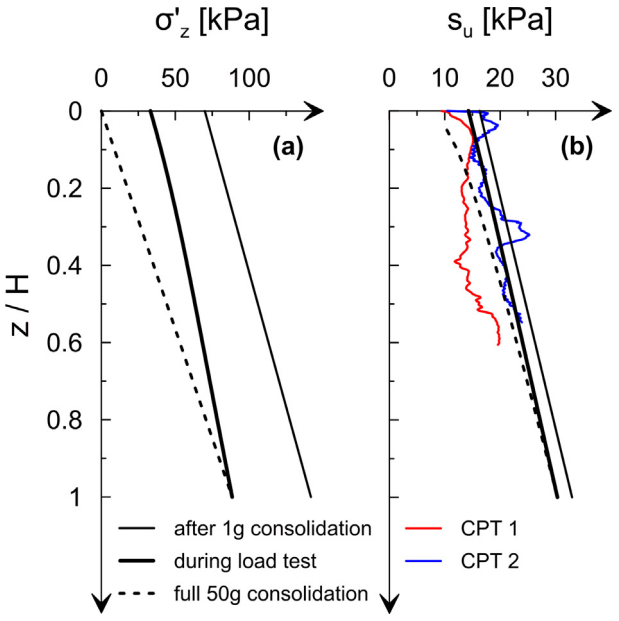

Fig. 4. Profile of (a) effective vertical stress at various stages in the test, and (b) theoretical and experimental undrained shear strength profiles.

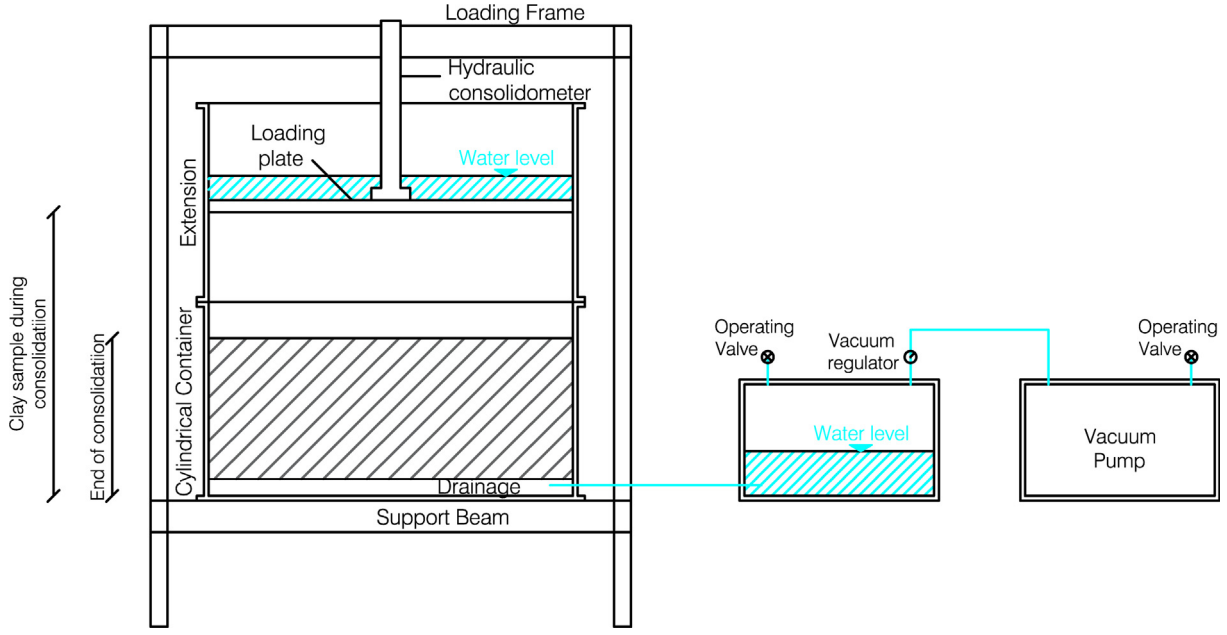

Fig. 3. Setup used for clay consolidation.

Fig. 5. Template raft for pile group installation.

All aluminium piles were coated with Houston sand (D_{50} = 0.356 mm), to simulate the contact of *cast-in-situ* reinforced concrete piles and were installed by pushing them in the clay layer at 1*g*. Since the piles are connected to the cap through spherical hinges, there was a risk that some of the piles may deviate from the vertical as the pile group was pushed into the clay. Therefore, the piles were driven using a template square raft, so that they could not rotate during installation (see Fig. 5). Before pile installation, the state of effective stress in the clay layer results from the combination of the load applied by the hydraulic press and the suction applied at the base, which is maintained due to suction in the clay. Installation will generate changes of effective stress and positive excess pore water pressures locally around the pile, which are not entirely straightforward to determine. However, the scope of the work was not to assess the effect of pile installation on the performance of isolated piles and pile groups, but rather to examine the response of pile groups under combined axial and moment loading to failure. Therefore, the response of isolated piles under tension and compression was determined experimentally to provide a term for comparison which includes installation effects.

The centrifuge models were instrumented to monitor soil and foundation response during the tests, as shown in the plan view of Fig. 6. The settlements of the founda-

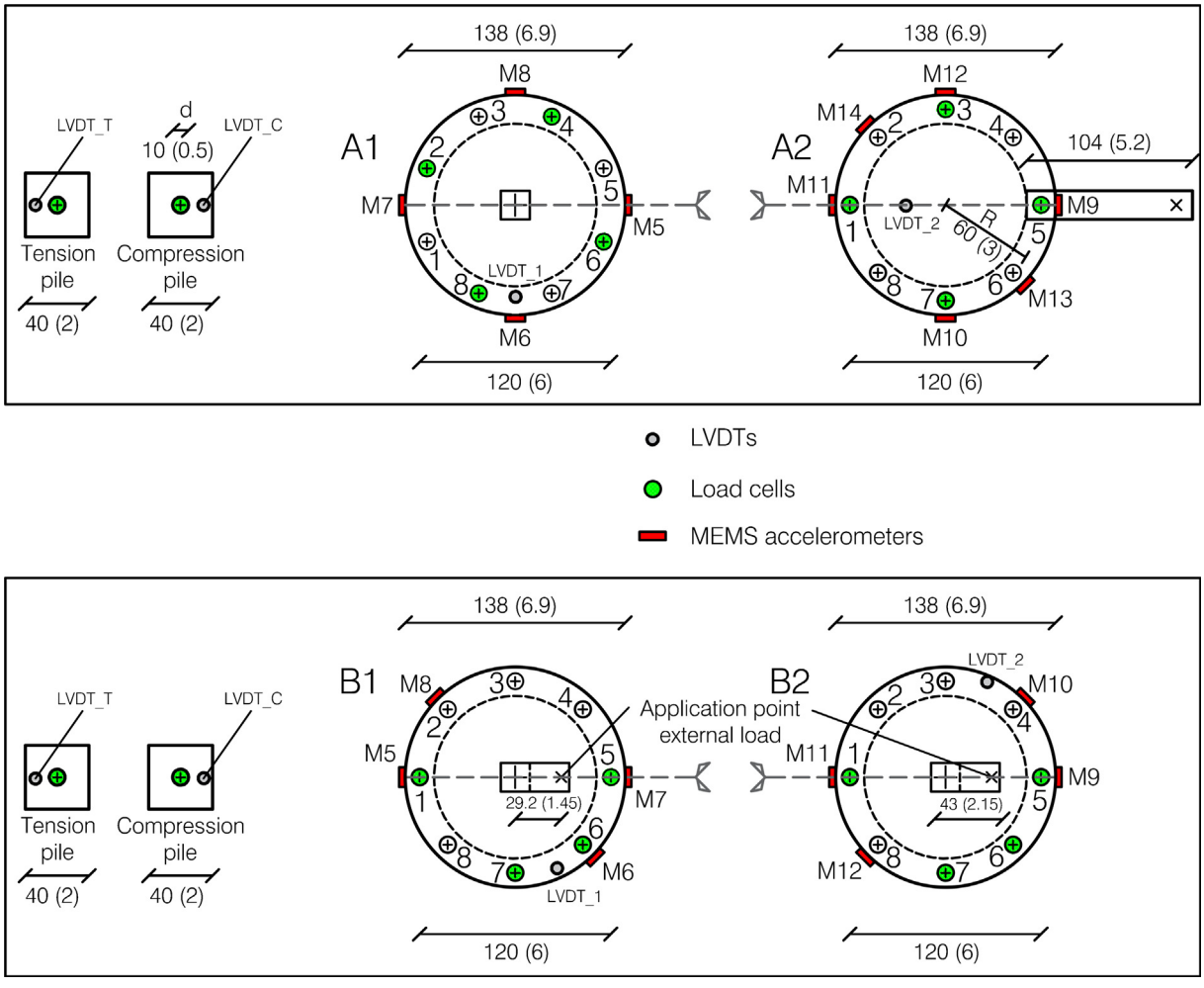

Fig. 6. Layout of monitoring devices adopted in the experiments; dimensions are given in mm at model scale, while dimensions in brackets (in m) refer to prototype scale.

tions were measured using vertically mounted Linear Variable Differential Transformers (LVDTs); the rotations of the rafts connecting the piles were measured using uniaxial Micro-Electro-Mechanical-Systems (MEMS) accelerometers; the axial loads of half of the piles were measured using miniaturised Load Cells (LCs) positioned immediately below the spherical hinges. Pore water pressures at different locations in the soil mass were recorded by means of miniature Pore Pressure Transducers (PPTs).

One LVDT was used to measure the vertical displacement of each raft, while the rotation of the rafts was measured using MEMS accelerometers. In the first set of experiments (Set A), the external load applied on the pile groups was evaluated indirectly from the available loads measured on individual piles, as detailed in the following. In the second set of experiments (Set B), load cells were mounted on the driving actuators, and, therefore, a direct measurement of the external load on the pile groups was available. The proposed layout has advantages over alternative, more sophisticated options:

- spherical hinges allow a direct and straightforward interpretation of the load distribution among piles, provided that the external moment cannot be but equilibrated by axial loads on piles;
- the circular raft connecting the piles can be idealized as a rigid body and, hence, very limited instrumentation is sufficient to evaluate the displacement of any pile during the entire loading history. These may include either two LVDTs measuring the vertical displacement of the raft at two points or, as in the present case, only one LVDT and a small number of MEMS accelerometers measuring the cap rotation.

2.2. Re-consolidation in the centrifuge and testing procedure

After removing the cylindrical container from the hydraulic press and the vacuum pump, the total vertical stress at the top of the clay layer drops to zero, while the effective vertical stress within the clay body remains unchanged, due to the development of negative excess pore water pressures. The required centrifuge acceleration of 50g was reached in 10g increments. The expected effective vertical stress profile at the end of the re-consolidation stage is plotted in Fig. 4a as a dashed line. The measurements recorded by the PPTs within the soil mass indicated that the excess pore water pressures induced by the application of the increased gravity in the centrifuge did not dissipate completely. The profile of effective vertical stress at the end of reconsolidation must therefore have been somewhere between the lines labelled 'after 1g consolidation' and 'full 50g consolidation', and can be computed using the classic solutions by Terzaghi (1943) for any given value of the degree of consolidation, U. Specifically, the profile of effective vertical stress can be estimated by combining the solutions for a rectangular shaped and a triangular shaped initial excess pore water pressure profiles dissipating only towards the base of the clay layer, because its upper surface behaves like an impermeable boundary. As an example, Fig. 4a shows the profile of effective vertical stress corresponding to a degree of consolidation $U = 70\%$. At the bottom of the clay layer, the effective vertical stress is equal to that expected at the end of consolidation, while the effective vertical stress at the top of the clay layer is intermediate between zero and the unit load applied by the hydraulic press. Fig. 4(b) shows the profiles of undrained shear strength, s_u, obtained from two Cone Penetration Tests (CPTs) carried out with a miniature CPT device, with a diameter of 6.35 mm and a 60° cone tip. CPT 1 (set A) was carried out at 1g after the swing down stage, whereas CPT 2 (Set B) was performed in flight after reconsolidation of the clay. The cone tip resistance (q_c) was converted into undrained shear strength, s_u, using the following equation:

$$s_u = \frac{q_c - \sigma_{v0}}{N_k} \tag{1}$$

where σ_{v0} is the total overburden stress and N_k is the cone factor ranging from 8 to 12 for smooth cones (Teh and Houlsby 1991). An average N_k of 10 is used in this study. The theoretical profile of s_u determined from critical state theory (Roscoe et al. 1958) using the parameters in Table 1 and the effective vertical stress profile in Fig. 4(a), corresponding to $U = 70\%$, is in very good agreement with the experimental profile of undrained shear strength obtained from CPT 2, but for very shallow depths where there is a small effect of surface drying. The above theoretical solution will be therefore taken as the reference profile for the interpretation of the experiments under examination.

A crucial point of the experimental procedure is the application of the load history to the model foundations. In all cases, the external load was applied under displacement control, by setting the displacement rate of the driving actuator at 1 mm/s. The displacements imposed by the actuators were large enough to allow a clear identification of the collapse load for all the examined models. The external load was applied on the end of the cantilever beam attached to the cap, through a half ball bearing, so that it could be idealized as a point load. The external load applied under displacement control has constant eccentricity and, hence, the direction of the load path in the (Q, M) plane is known *a-priori*; this allows to identify the moment load corresponding to the collapse of the group.

Fig. 7 shows the initial configuration of the foundation model subjected to positive (compressive) vertical load with high eccentricity (Set A). It is easy to distinguish some important details in this figure, such as the cantilever beam, the half ball bearing for the application of the point load, the pile layout, the load cells on some of the piles, and the miniature CPT. Fig. 8 shows the final configuration achieved for the pile group tested in tension under small eccentricity (Set B). As mentioned before, in this case, a

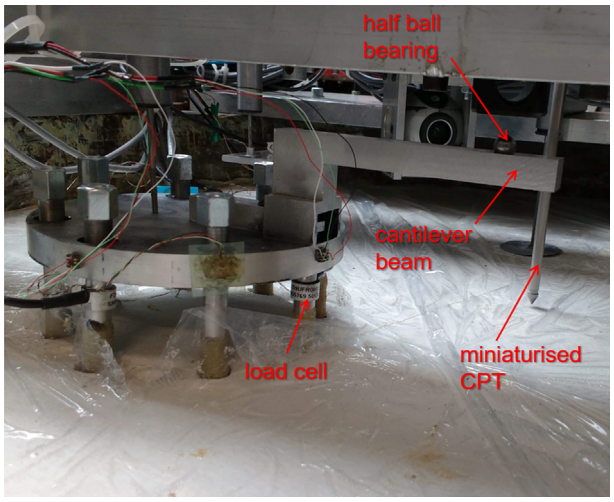

Fig. 7. Foundation model for loading test in compression under high eccentricity.

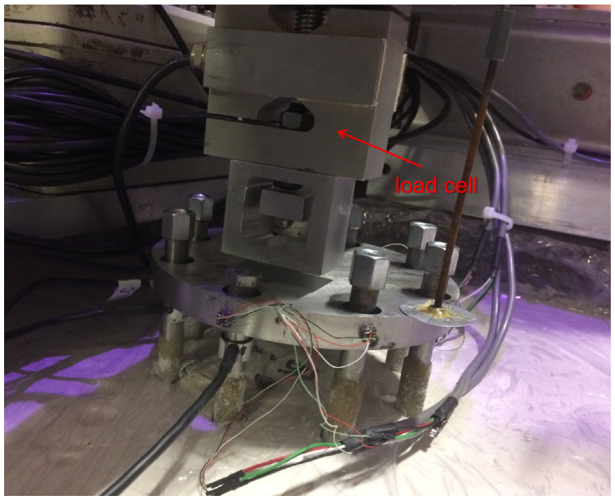

Fig. 8. Foundation model for loading test in uplift under small eccentricity.

load cell is mounted on the driving actuator, to measure directly the applied vertical load, and the raft is lifted by a square ring attached to the load cell and acting on a spherical device positioned on the lower face of the cantilever beam.

3. Experimental results

Results from the miniature CPTs were discussed before. The focus is now set on the load-settlement response of the model foundations. Based on previous experience, a sampling frequency of 5 Hz is sufficient for an accurate representation of monitoring data.

Table 2 provides the masses of the isolated piles, the pile groups and the circular rafts at model scale. The masses reported in the table are those of sand coated piles. The

Table 2
Masses of foundation elements at model scale (kg).

Component	Set A	Set B
Isolated pile in tension	0.120	0.120
Isolated in compression	0.115	0.117
Piles of group 1- total	0.680	0.688
Connecting cap for pile group 1	0.382	0.440
Piles of group 2 – total	0.665	0.670
Connecting cap for pile group 2	0.485	0.430

mass of the raft includes the contribution of the cantilever beam for the application of the eccentric load.

As shown in Fig. 6, the pile groups subjected to eccentric load were equipped with MEMS accelerometers. Two of these (M13 and M14) were positioned with their sensitive axis parallel to soil surface, while all the remaining MEMS accelerometers had their sensitive axis oriented along the vertical direction. In this case, the rotation at any instant of time can be expressed as:

$$\theta(t) = \arccos\frac{a(t)}{a_0} \tag{2}$$

where a(t) is the acceleration recorded by the MEMS accelerometer at any time and a_0 is the acceleration before the application of the external load. On the other hand, for the two horizontally oriented MEMS accelerometers, the rotation is evaluated as:

$$\theta(t) = \arcsin\frac{a(t)}{N\sin\beta} - \arcsin\frac{a_0}{N\sin\beta} \tag{3}$$

in which β is the angle in the horizontal plane between the sensitive axis of the MEMS accelerometer and the conjunction line between piles 3 and 7 (see Fig. 6), and N is the current ratio between the acceleration in the model and the earth gravity acceleration. The acceleration field within the centrifuge model varies linearly with the distance r from the centre of rotation (Madabhushi, 2014):

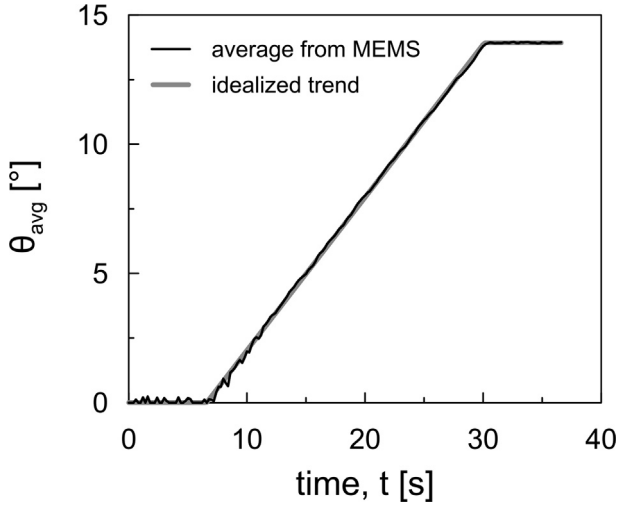

Fig. 9. Time history of the average value of the rotations recorded by MEMS glued on cap of pile group A2.

$$Ng = r\omega^2 \quad (4)$$

in which ω is the angular speed of the centrifuge and Ng is the centrifuge acceleration. As an example, Fig. 9 illustrates the time history of the average value of the rotations recorded by MEMS accelerometer glued on the cap of pile group A2 during the test. Finally, the centrifuge acceleration 'Ng' values at the elevation of the rafts connecting the piles are fully consistent with accelerations recorded by the MEMS accelerometers.

All data will be presented at the prototype scale in the following.

3.1. Isolated single piles

Fig. 10 illustrates the load settlement curves from loading tests in compression and tension on isolated piles. The results from the two loading tests in compression are in relatively good agreement. The difference between the peak values of the applied external load is less than 10%, with the isolated pile of set B exhibiting a slightly larger resistance. For piles in tension, the agreement between the results from the two tests is still satisfactory, even if the difference between the two peak values of the external load in this case is larger, about 15%. This can be attributed to the variability of the shaft capacity of piles coated with sand; as the capacity in compression includes also end bearing capacity, the behaviour in compression is less affected by the variability of the shaft capacity. While piles in compression exhibit minor softening, the tension capacity of isolated piles reduces significantly in the post-peak stage, which further confirms the larger role played by the shaft resistance on the overall capacity of the pile.

For all tested pile foundations and irrespective of whether the pile was tested in compression or extension, the vertical displacement at which the axial capacity is mobilized is about 10% of the diameter of the pile. This value is in agreement with that suggested by Fleming et al. (2008) and Viggiani et al. (2012) for piles in compression. However, about the same value of vertical displacement, *i.e.* 50 mm, is needed to mobilize the shaft capacity in tension. As outlined by Viggiani et al. (2012), the displacement needed to mobilize the maximum shaft capacity in compression is almost independent of the pile diameter and equal to about 20 mm. This discrepancy is not surprising. In fact, as the initial shear stresses on the shaft are of opposite sign compared to those occurring when the capac-

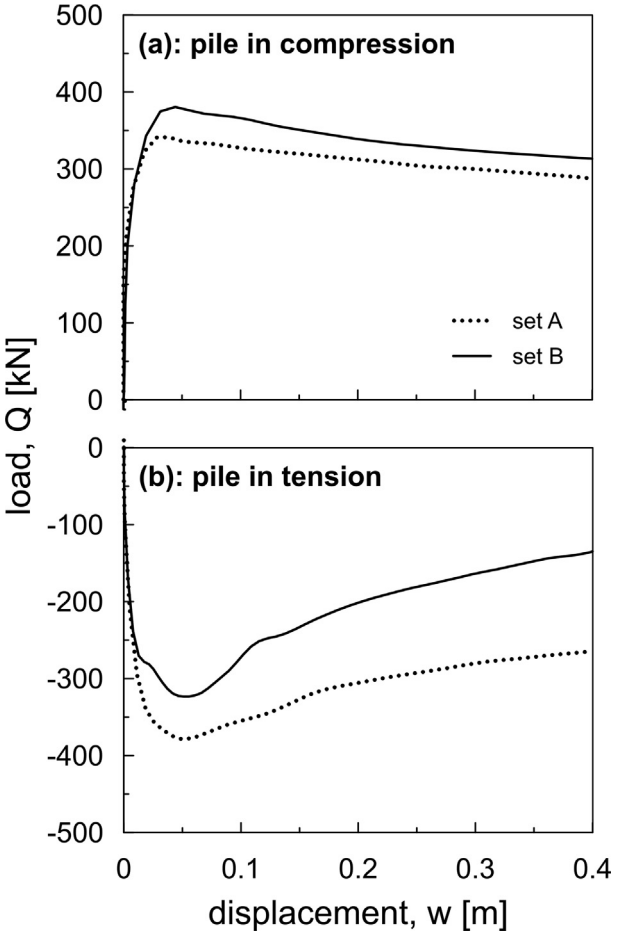

Fig. 10. Load settlement response of isolated piles in compression and in tension.

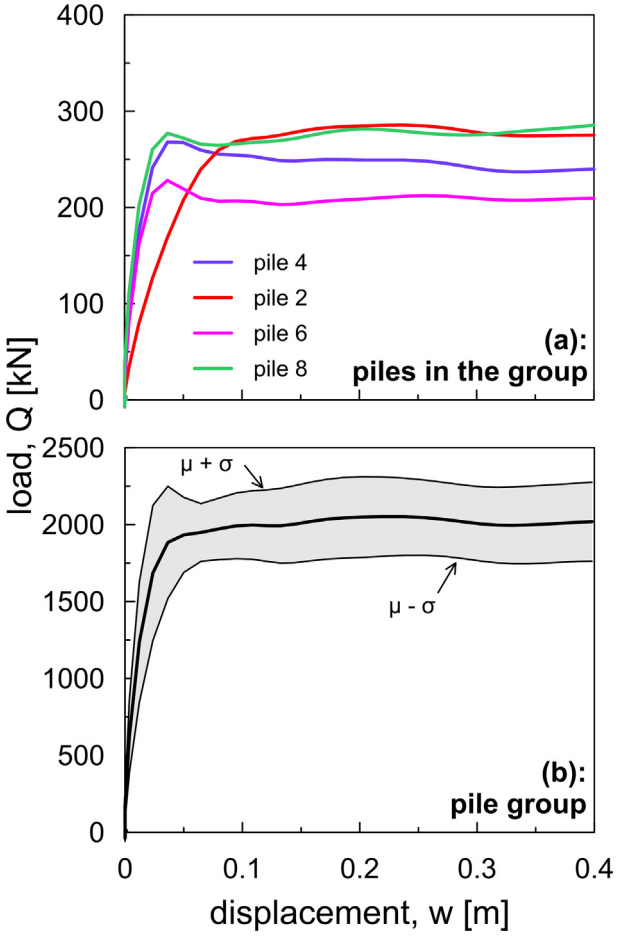

Fig. 11. A1: Pile group under centered load: (a) load displacement curves of piles equipped with load cells; (b) load settlement response of the group.

ity in tension is mobilized, the absolute upward displacement needed to achieve the failure load in tension must be much larger than the downward displacement mobilizing the shaft capacity in compression.

3.2. Pile groups

For pile group A1, subjected to centred vertical load, the driving actuator was not equipped with a load cell, so that the external load acting on the group was not measured directly. The external load is equilibrated by the axial loads on individual piles, but only half of the piles belonging to the group were fitted with load cells (see Fig. 6). It is reasonable to assume that the load distribution in the piles would be symmetric about the line indicated in Fig. 6, and, therefore, the total load on the pile group at any time can be computed as:

$$Q(t) = 2\sum Q_i \tag{5}$$

where Q_i is the load acting on i^{th} instrumented pile.

Fig. 11(a) illustrates the load settlement response of the piles instrumented with LCs. The capacities of the individual piles are all very similar, with maximum recorded loads ranging between 229 kN and 287 kN. However, while piles No. 4, 6, and 8 reached their capacity at an axial displacement of about 36 mm, or 7.2% of the diameter of the pile, and then exhibited softening, pile No. 2 reached capacity at a larger displacement, of the order of 20% of the pile diameter, or 100 mm. The compliant behaviour of pile No. 2 testifies to slackness in the system, including the screw connection between the load cell and the pile.

In order to take into account the variability of axial load on piles, the results from all four instrumented piles were used to compute the mean and standard deviation of the axial loads carried by the piles at each given vertical displacement. For instance, at a displacement of 0.04 m, corresponding to the peak loads of piles 4, 6 and 8, $\mu = 235$ kN and $\sigma = 46$ kN, so that the Coefficient of Variation (CoV) is about 0.2. Fig. 11(b) shows the total load carried by the pile group (thick line) together with the curves corresponding to plus or minus one standard deviation. The total load carried by the group and the standard deviation are computed as eight times the average load and standard deviation on single piles, respectively. The sum of the axial loads recorded by all the load cells remains almost constant for displacements larger than 0.04 m.

For pile group A2, subjected to eccentric load, even if the distribution of load is taken to be symmetrical with respect to the plane containing the external moment load, it is not possible to know the axial loads on piles No. 4 and 2 (or, equivalently No. 6 and 8), not fitted with load cells (see Fig. 6). The applied total external load and moment are also unknown quantities, even if they have to satisfy the following relationship:

$$M = Qe \tag{6}$$

where e is the eccentricity of the point load, equal to 7.25 m at prototype scale. Since there are 4 unknown quantities and three equations, namely moment and force equilibrium and Eq. (6), the problem is indeterminate. In the interpretation of the results, we assumed that:

$$Q_4(t) = Q_5(t)\ [Q_6(t) = Q_5(t)] \tag{7}$$

This is reasonable because the alignment of piles 4-6 is very close to pile 5 and all these piles are subjected to (positive) compression loads. The indeterminate quantities reduce therefore to Q_2 (or Q_8), Q and M. Fig. 12 shows the load-rotation response of the pile group computed under the assumption in Eq. (7) together with the load settlement curves of the instrumented individual piles. Because the external load is applied under constant eccentricity, the quantity on the y-axis of Fig. 12 is also representative of the applied external moment M, see Eq. (6). This is plotted against θR, where R is the radius of the circle through the centres of the piles, to obtain a nominal displacement comparable to the displacements of individual

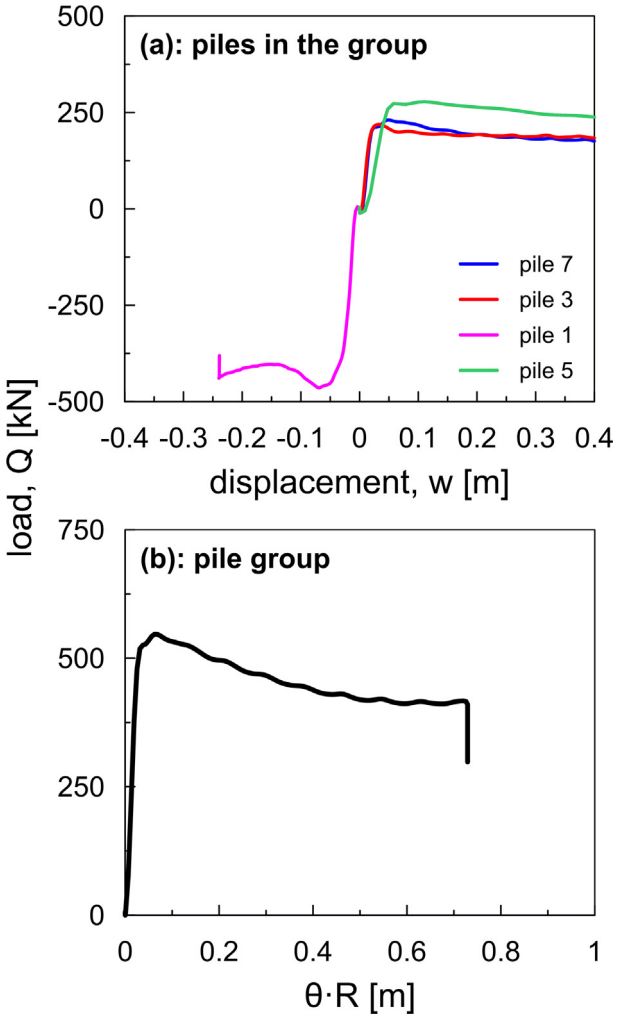

Fig. 12. A2: Pile group under vertical, high eccentric load: (a) load-settlement curves of piles fitted with load cells; (b) load-rotation curve for the pile group.

piles. The settlement of any pile belonging to the group was evaluated by the displacement recorded by the LVDT mounted on the cap, w_0, and the average value of the rotations recorded by the MEMS, θ:

$$w_i = w_0 - \theta(x_i - x_0) \tag{8}$$

where x_i and x_0 are the abscissas of the i-th pile and of the LVDT. In this case, the rotations recorded by all the MEMS were very similar and their average final value matched exactly the rotation measured manually using a tilting device at the end of the test. Piles 3 and 7 exhibit practically the same response, giving confidence that the assumption about the plane of symmetry along piles 1–5 is appropriate in this case. All piles under compression mobilized their capacity at a settlement of about 10% of the pile diameter. The peak compression load falls in a quite narrow band (219 kN to 278 kN), while the maximum value of the tension load on pile 1 is −465 kN. Overall, the moment-rotation response exhibits significant softening, as the moment capacity reduces by 25% after the achievement of the peak value.

Pile group B1 was subjected to compression load with small eccentricity. As mentioned before, the driving actuators of the pile groups in Set B were fitted with load cells, so there is no need to evaluate the time history of the external load by summing the axial loads on individual piles. However, the sum of the axial loads on individual piles can be compared to the total load measured at the actuator to check the assumptions on the load distribution among piles. As before, assuming a plane of symmetry along piles 1–5, the unknown quantities reduce to the external load and the axial load on pile 2 (or equivalently pile 8, see Fig. 6); these can be computed by force and moment equilibrium. Fig. 13b shows the total load obtained using this procedure and the total load measured by the load cell mounted on the actuator as a function of rotation. The agreement between the two plots is generally very good, increasing the confidence on the assumption of symmetry for the distribution of axial loads on piles. The peak of the two curves, point (a), takes place at the same time, even if the two peak values differ by about 15%. This difference is fully compatible with the variability in axial capacity measured for group A1 subjected to centred load, see Fig. 11b. The difference between the two plots at very large rotations, between points (b) and (c) is due to the load cell on the actuator coming into contact with the cantilever beam used to apply the eccentric load. Also shown in Fig. 13a are the load displacement plots for the individual piles within the group. While the loads recorded by the individual load cells provide reliable measurements of the capacity of the piles, in this case the rotations recorded by the MEMS were very erratic. It follows that the axial displacements of individual piles were problematic to compute using Eq. (8), which resulted in unreliable load-settlement curves. The plots for piles 5 and 6, in compression, are very similar and relatively convincing, whereas the plots for pile 7 in compression and pile 1 in tension are very irregular and difficult to interpret.

Fig. 14 shows the experimental data from the test on pile group B2, subjected to a tensile load with a small eccentricity. In this test, pile 1 is loaded in compression (positive) while all the remaining piles are subjected to tensile (negative) loads. As for pile group B1, the rotations recorded by the MEMS were very erratic rendering the computed displacements of individual piles unreliable and, therefore, the interpretation of their load-settlement response problematic, even if the loads recorded by individual load cells permitted to measure the capacities of individual piles. Fig. 14b compares the external load computed from the individual loads on piles using the symmetry criterion with that recorded by the load cell mounted on the actuator. The agreement between the two curves is extremely good until a critical value of the cap rotation, at point (b), at which collapse has already occurred and the square ring mounted on the load cell to pull the group comes in contact with the cantilever beam.

4. Interpretation of loading tests on foundation models

4.1. Isolated piles

The axial capacity of the isolated piles is determined from the plots in Fig. 10. The capacity of the isolated pile in compression can be computed as:

$$N_u = Q_{\max} + W \tag{9}$$

where $Q_{\max}$ is the peak value of the external load and W is the weight of the capped pile, including the small square raft. The capacity in tension is instead calculated as:

$$-S_u = Q_{\min} + W \tag{10}$$

where $Q_{\min}$ is the minimum (negative) value of the applied load.

Table 3 summarizes the axial capacities derived from loading tests on isolated piles for Sets A and B. Historically, the shaft friction around a pile shaft has been estimated in terms of the s_u, according to the expression (Tomlinson 1957, Fleming et al. 2008):

$$s_{\lim} = \alpha \cdot s_u \tag{11}$$

where α is an empirical coefficient, also referred to as 'adhesion', depending not only on the shear strength of soil, but also on its past stress history and overconsolidation ratio (Randolph & Wroth 1981). This coefficient can be easily back-figured from the tension capacity of the pile and the theoretical profile of undrained shear strength in Fig. 4; which is 0.64 for Set A and 0.49 for Set B, as an average. The former value is in agreement with the recommendation of Viggiani (1993) for replacement piles in clay with undrained shear strength lower than 25 kPa ($\alpha = 0.7$), while the latter value is very close to the one suggested by O'Neill & Reese (1999) for replacement piles and $s_u \leq 150$ kPa ($\alpha = 0.55$).

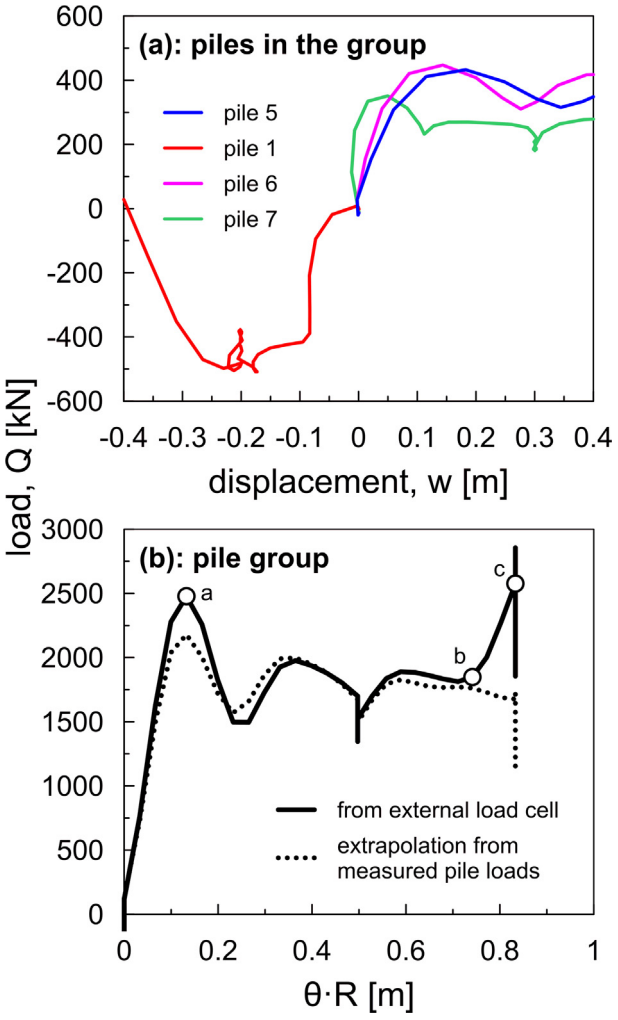

Fig. 13. B1: Pile group under compressive load with small eccentricity: (a) load-settlement curves of piles equipped with load cells; (b) load-rotation curve for the pile group.

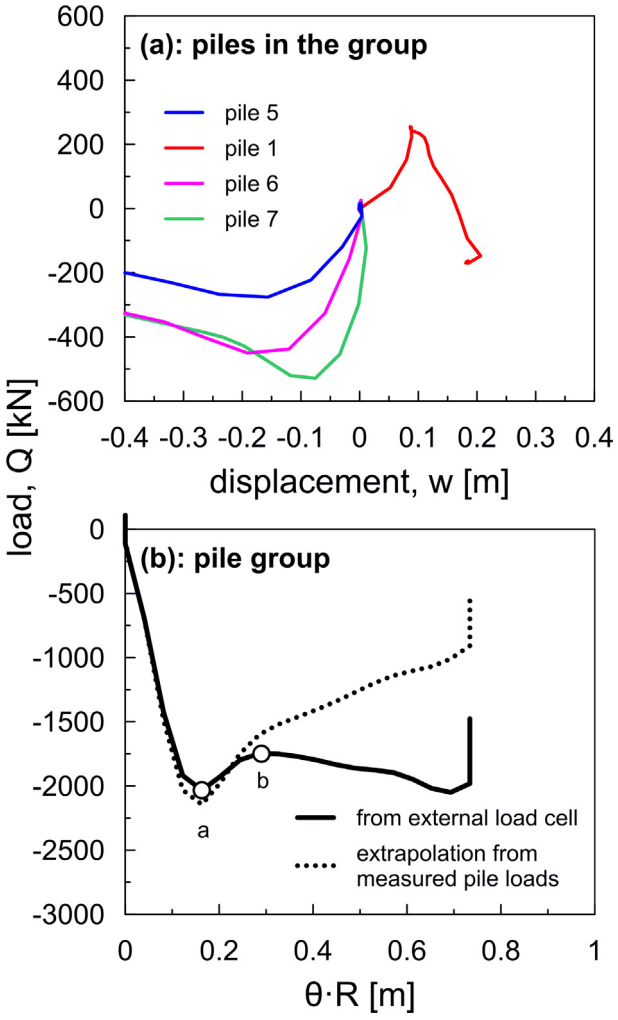

Fig. 14. B2: Pile group under tension load with small eccentricity: (a) load-settlement curves of piles equipped with load cells; (b) load-rotation and load-average settlement curves for the pile group.

Because the load displacement curves of individual piles are nonlinear, a problem arises for the definition of their axial stiffness. In the following, the axial stiffness is referred to as the secant value corresponding to a displacement of 2% of the pile diameter, or 10 mm, which is still significantly smaller than the displacement corresponding to the attainment of the axial capacity, or about 10% of the pile diameter. Table 3 summarises the computed axial stiffness of the isolated piles.

4.2. Pile groups

For pile groups A1, A2 and B1, the ultimate axial load is evaluated as:

$$Q_u = Q_{\max} + W_{piles} + W_{cap} \tag{12}$$

where $Q_{\max}$ is the first peak of the compression load, W_{piles} is the weight of the piles and W_{cap} is the weight of the raft connecting the piles. This last quantity includes the contribution of the cantilever beam for pile groups A2 and B1.

On the other hand, for pile group B2, the tension capacity is calculated as:

$$Q_u = Q_{\min} + W_{piles} + W_{cap} \tag{13}$$

where $Q_{\min}$ is the first (negative) peak achieved during the test. As outlined before, the gravity field in the centrifuge model varies linearly with the distance from the centre of rotation, according to Eq. (4). As a result, the value of acceleration (Ng) at the elevation of the cap is smaller than the reference acceleration of 50g. While the weight of piles was computed by assuming an increased gravity of 50g, the weight of the circular raft was calculated by taking the exact value of the scale factor N corresponding to the cap elevation in the centrifuge model. The moment capacity of a pile group is defined as the external moment applied to the foundation model corresponding to Q_u. For pile group A1, subjected to centred load, the moment capacity is obviously zero. By contrast, for pile groups A2 and B1, the ultimate moment is evaluated through the following equation:

Table 3
Axial capacity and axial stiffness in compression and uplift of isolated piles.

Test	Set	$Q_{max}[Q_{min}]$ (kN)	$N_u[-S_u]$ (kN)	W (kN)	$K_c[K_t]$ (MN/m)
compression	A	341	455	114	28
[tension]	A	−379	−267	112	28
compression	B	381	496	115	28
[tension]	B	–323	−204	119	25

$$M_u = M_0 + Q_{\max} \cdot e = W_{beam} \cdot e_0 + Q_{\max} \cdot e \quad (14)$$

in which M_0 is the moment generated by the weight of the cantilever beam, e_0 is the eccentricity of W_{beam} and e is the eccentricity of the external load. At the same time, for the pile group subjected to tension, the moment capacity is computed as:

$$M_u = M_0 + Q_{\min} \cdot e = W_{beam} \cdot e_0 + Q_{\min} \cdot e \quad (15)$$

where, once again, $Q_{\min}$ is a negative quantity.

The definition of the capacity of the group required careful inspection of the load displacement plots from individual piles as detailed in the following. For the pile group under centred load only, pile group A1, we take $Q_{\max}$ as the load corresponding to time at which the axial capacity of piles 4, 6, and 8 is fully mobilized. Such value does not correspond to the first peak of the loading history, but it is clearly associated to the occurrence of collapse, as shown in Fig. 15a. Noticeably, this value corresponds to the point of maximum curvature of the load settlement plot in Fig. 11b. As an alternative, the collapse may be taken at time corresponding to the first local maximum of the entire load history. In case of pile group A2, the first local maximum of the entire load history takes place when the axial capacity of outermost pile No. 5 has been already mobilized, as it can be argued from Fig. 15b. At the same instant, the opposite outermost pile has not yet mobilized its tension capacity. For pile group B1, the foundation attains the first local maximum almost simultaneously with the mobilization of the axial capacity in compression of piles 5, 6 and 7; at the same instant time, pile 1 under tension load has not achieved the tension capacity, as per pile group A1, see Fig. 16a. Finally, for pile group B2, the instant time at which the collapse occurs, the outermost pile in tension (No. 5) has already mobilized its tension capacity (Fig. 16b).

The ultimate coordinates (Q_u, M_u) of the pile groups tested in the centrifuge are summarised in Table 4. The load paths followed in the centrifuge are also represented in Fig. 17 for all the model foundations. Noticeably, the initial moment due to the cantilever beam is about 10% of the ultimate moment for pile group A2, while it is negligible for the foundation models belonging to Set B. The moment capacity is strongly affected by the axial load applied on the foundation model; for compressive (positive) loads, the smaller the eccentricity of the axial force the lower the ultimate moment of the pile group. The moment capacity of pile group B1, subjected to a compression load with eccentricity of 1.45 m is comparable to that recorded of pile group B2, where the axial force has the same eccentricity but opposite sign. The failure domain based on the conventional approach, in which the collapse of the foundation is identified with the achievement of the axial capacity in tension or compression on the outermost pile, is also shown for comparison. The collapse domain is evaluated for both series of experiments from the axial capacities of the isolated piles, see Table 3. The (Q, M) values such that the outermost pile fails in compression or uplift will satisfy the set of equations:

$$M = \mp \frac{a^2}{nR} Q \pm \frac{a^2 N_u}{R}$$
$$M = \pm \frac{a^2}{nR} Q \pm \frac{a^2 S_u}{R} \quad (16a, b)$$

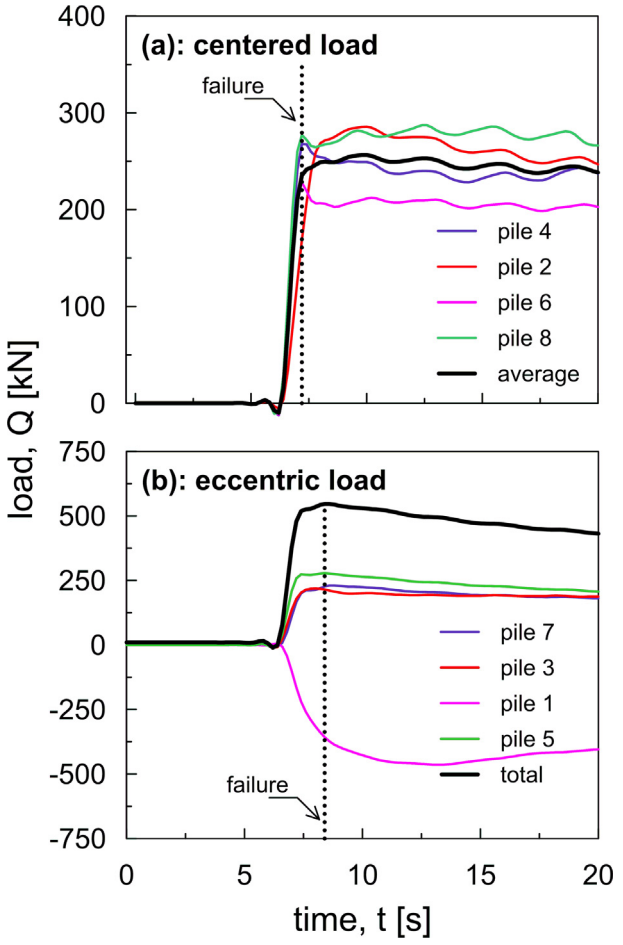

Fig. 15. Set A – load histories from LCs: (a) pile group A1; (b) pile group A2.

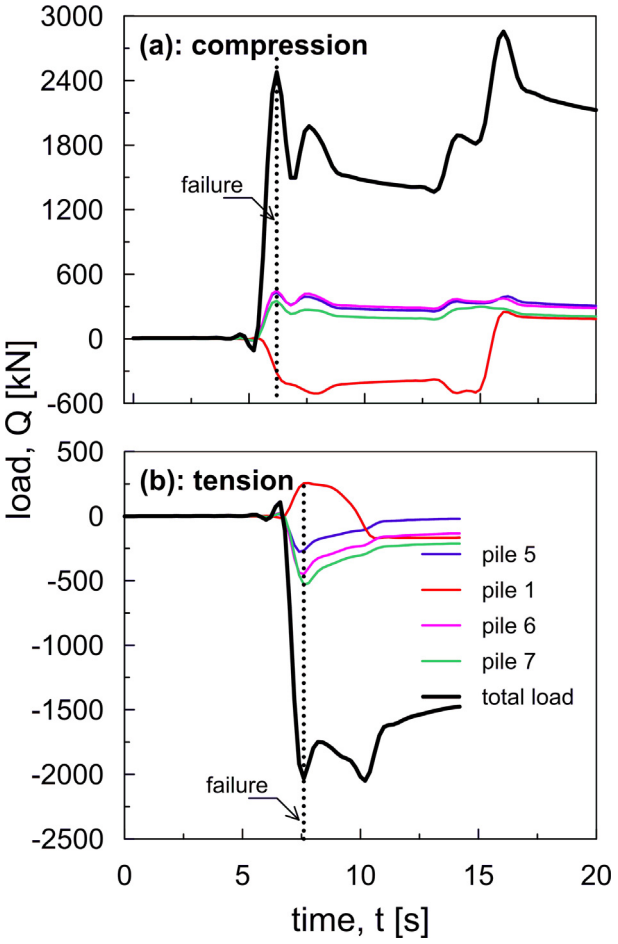

Fig. 16. Set B – load histories from LCs: (a) pile group B1; (b) pile group B2.

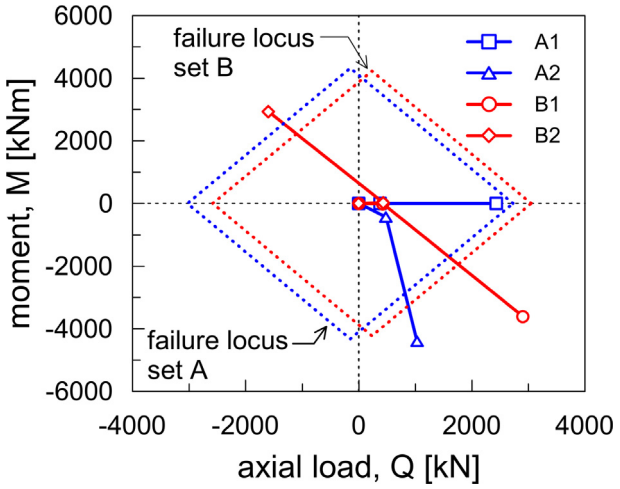

Fig. 17. Load paths followed in the centrifuge and conventional failure domains.

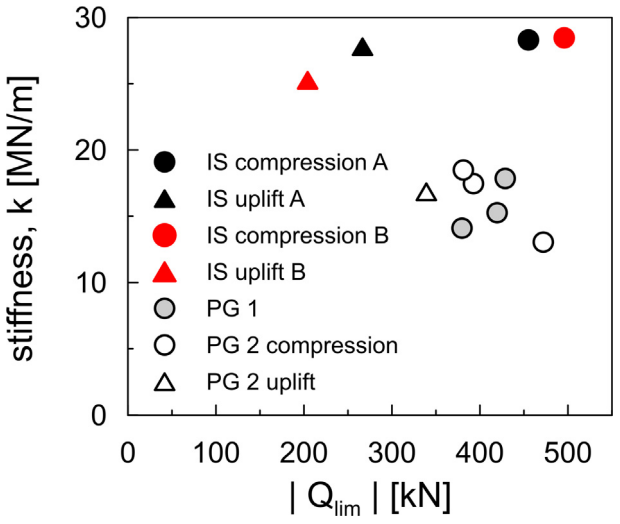

Fig. 18. Axial stiffness vs. axial capacity for piles within the groups.

where the first option about the sign corresponds to the case of counter-clockwise moment and the second option to a clockwise moment, while

$$a^2 = \sum_{i=1}^{n} x_i^2 \tag{17}$$

in which x_i is the abscissa of the i-th pile relative to the centre of the foundation. Eqs. (16a, b) are four linear relationships between moment and axial load identifying a rhombus in the (Q, M) plane. They derive from the assumption that axial loads on the piles are distributed linearly, which for rectangular groups is not satisfied due to pile-to-pile interaction (group effects). However, in the case of annular shaped pile groups, Eqs. (16a, b) are rigorous even if pile-to-pile interaction effects are explicitly taken into account. The distance of the endpoints of the load paths followed in the centrifuge from the boundary of the conventional failure domain is paradigmatic of the level of conservatism of current industry-based design methods.

Finally, the axial stiffness of piles within the groups in set A is considered. The secant axial stiffness defined according to the same procedure followed for isolated piles is plotted in Fig. 18 as a function of the axial capacity in compression or tension. The axial stiffness of isolated piles is about 1.5–2 times that of piles in the group. The pre-load

Table 4
Ultimate axial-moment coordinates from the experiments on pile groups.

Load path	Set	e (m)	W_{piles} (kN)	W_{cap} (kN)	M_0 (kNm)	Q_{ext} (kN)	Q_u (kN)	M_u (kNm)
Centered	A	0	834	379	0	2141	3354	0
Eccentric	A	7.25	815	481	440	547	1843	4402
Eccentric	B	1.45	822	424	14	2478	3724	3608
Eccentric	B	1.45	840	433	17	−2033	−759	−2930

on piles within the group is larger than that on isolated piles, because of the contribution of the raft, so that the degree of mobilization of the lateral capacity is greater for piles within the group. Moreover, group effects, as defined by Poulos (1968) and Butterfield & Banerjee (1971), affect the behaviour of piles within the group. These two factors contribute to a softer response of the piles in the group.

5. Discussion and conclusion

In this study, the results of a centrifuge testing program on models of annular-shaped pile groups embedded in clay were presented with the aim of investigating the bearing behaviour of this kind of foundation under vertical, eccentric load. Two series of centrifuge experiments on reduced scale models of pile groups were carried out using monotonic loading paths under constant eccentricity or constant axial load. The raft is clear of the soil and the connection between piles and raft is hinged. Each series included also two tests on isolated piles, one in compression and one in tension.

The experimental procedure followed in this work permitted to identify clearly the response of the examined foundations until the achievement of a collapse mechanism. It was shown that the ultimate moment depends strongly on the slope of the load path in the (Q, M) plane, *i.e.*, on the eccentricity of the applied load. Under compression (positive) load, the smaller the eccentricity the lower is the moment capacity of the pile group. Pile-to-pile interaction effects deduced from the comparison between the axial stiffness of isolated piles and that of piles within the groups are particularly relevant, as it was expected. Piles belonging to annular groups subjected to moment loading respond in a stiffer manner than piles belonging to the pile group under centred load, due to the fact that group effects are less pronounced when tension and compression loads on piles act simultaneously. The above results should be taken in due consideration to improve ultimate capacity and settlement performance criteria of piled foundations under combined axial-moment loads.

As outlined in the introduction, the data supplied in this work may serve as a benchmark to validate the performance of mathematical models aimed at predicting the bearing behaviour of piled foundations in the (Q, M) plane. Also, the experimental procedure illustrated in this work may be conveniently adopted to explore the response of pile groups under load paths other than those examined in the paper.

Acknowledgments

This work has been carried out under a research agreement between University of Napoli Parthenope and the Italian multinational for renewable energies corporation Enel Green Power.

References

AASHTO, L., 2012. AASHTO LRFD bridge design specifications.

Banerjee, P.K., Driscoll, R.M., 1976. Three-dimensional analysis of vertical pile groups. ha Proceedings, Second International Conference on Numerical Methods in Geomechanics, pp. 438–450.

Butterfield, R., Banerjee, P.K., 1971. The problem of pile group–pile cap interaction. Geotechnique 21 (2), 135–142.

Clancy, P., Randolph, M.F., 1993. An approximate analysis procedure for piled raft foundations. Int. J. Numer. Anal. Meth. Geomech. 17 (12), 849–869.

de Sanctis, L., Russo, G., 2008. Analysis and performance of piled rafts designed using innovative criteria. J. Geotech. Geoenviron. Eng. 134 (8), 1118–1128.

Di Laora, R., de Sanctis, L., Aversa, S., 2019. Bearing capacity of pile groups under vertical eccentric load. Acta Geotech. 14 (1), 193–205.

Kishida, H., Meyerhof, G.G., 1965. Bearing capacity of pile groups under eccentric loads in sand. Proc. 6th ICSMFE. Montreal 2, 270–274.

Fleming, W.G.K., Weltman, A.J., Randolph, M.F., Elson, W.K., 2008. Piling engineering. CRC Press.

Garala, T.K., Madabhushi, S.P.G., 2019. Seismic behaviour of soft clay and its influence on the response of friction pile foundations. Bull. Earthq. Eng. 17, 1919–1939.

GWEC (Global Wind Energy Council), 2015. Global wind report: Annual market update 2015. Brussels.

Lau, B.H., 2015. Cyclic Behaviour of Monopile Foundations for Offshore Wind Turbines in Clay PhD dissertation. University of Cambridge, Cambridge, UK.

Liebreich, M., 2017. State of the Clean Energy Industry. The 'Future of Energy' Summit, Bloomberg New Energy Finance, London, Sept. 2017.

Madabhushi, G., 2014. Centrifuge Modelling for Civil Engineers. CRC Press.

Meyerhof, G.G., 1981. The bearing capacity of rigid piles and pile groups under inclined loads in clay. Can. Geotech. J. 18 (2), 297–300.

Meyerhof, G.G., Ranjan, G., 1973. The bearing capacity of rigid piles under inclined loads in sand. III: Pile Groups. Can. Geotech. J. 10 (3), 428–438.

Meyerhof, G.G., Yalcin, A.S., 1984. Pile capacity for eccentric inclined load in clay. Can. Geotech. J. 21 (3), 389–396.

Meyerhof, G.G., Yalcin, A.S., Mathur, S.K., 1983. Ultimate pile capacity for eccentric inclined load. J. Geotech. Eng. 109 (3), 408–423.

O'Neill, M.W., Reese, L.C., 1999. Drilled shafts: construction procedures and design methods. Publication No. FHWA-IF-99-025, Federal Highway Administration, Washington, DC, 758 pp.

Poulos, H.G., 1968. The behaviour of a rigid circular plate resting on a finite elastic layer. Civil Eng. Trans., Instn. Engrs., Austin, Texas 10, 213–219.

Randolph, M.F., Wroth, C.P., 1981. Application of the failure state in undrained simple shear to the shaft capacity of driven piles. Geotechnique 31 (1), 143–157.

Ravichandran, N., Shrestha, S., Piratla, K., 2018. Robust design and optimization procedure for piled-raft foundation to support tall wind turbine in clay and sand. G_{max}-qc Relationships for Clays. Soils Found. 58, 744–755.

Roscoe, K.H., Schofield, A.N., Wroth, C.P., 1958. On the yielding of soils. Géotechnique 8 (1), 22–52.

Russo, G., Viggiani, C., 1998. Factors controlling soil-structure interaction for piled rafts. Darmstadt Geotech. Darmstadt. Univ. Technol. 4, 297–322.

Saffery, M.R., Tate, A.P.K., 1961. Model tests on pile groups in a clay soil with particular reference to the behaviour of the group when it is loaded eccentrically. Proceedings of the Fifth Conference on Soil Mechanics and Foundation Engineering, pp. 129–134.

Shrestha, S., 2015. Design and Analysis of Foundation for Onshore Tall Wind Turbines M.S. thesis. Clemson University, Clemson, SC, USA.

Teh, C.I., Houlsby, G.T., 1991. An analytical study of the cone penetration test in clay. Geotechnique 41 (1), 17–34.

Terzaghi, 1943. Thoeretical Soil Mechanics. John Wiley & Sons, New York.

Tomlinson, M.J., 1957, August. The adhesion of piles driven in clay soils. In: Proceedings of the 4th International Conference on Soil Mechanics and Foundation Engineering, vol. 2, pp. 66–71.

Viggiani, C., 1993. Further experiences with auger piles in Naples area. Deep Found. Bored Auger Piles, 445–455.

Viggiani, C., Mandolini, A., Russo, G., 2012. Piles and Pile Foundations. CRC Press.